DOI 10.4430/bgo00384

Geoelectrical modelling of a landslide surface through an unstructured mesh

K. Damavandi, M. Abedi, G.-H. Norouzi and M. Mojarab

Petroleum Engineering and Geophysics Laboratory, School of Mining Engineering, Faculty of Engineering, University of Tehran, Iran

(Received: 4 July 2021; accepted: 10 December 2021; published online: 8 June 2022)

ABSTRACT Mass movements in wavy topographic zones pose a constant danger to infrastructure, water management, plantation formation, and human life. A commonly used method in near-surface geophysical surveys is Electrical Resistivity Tomography (ERT) to define various strata levels and calculate the likely slip surface of landslides. We use a developed algorithm named ResIPy to be able to incorporate surface topography using triangular cells in finite element forward and inversion processes. Initially, a synthetic landslide case demonstrates that employing the triangular mesh results in more accurate identification of the geological formations than the rectangular mesh, which requires more CPU time. Then, field data from a prone landslide at approximately 20 km NW of the Tehran province, in Iran, was investigated using eight geoelectrical profiles spaced 20 m along the sliding surface accompanying one borehole. The sliding surface corresponds to a deep zone with low resistivity due to the presence of shale, and the sliding material is composed of gravelly soil, silt, and tuff. According to the field observations, the crown portion is vulnerable to sliding because there are transverse cracks in the uphill slope.

Key words: electrical properties, Electrical Resistivity Tomography (ERT), numerical solutions, unstructured mesh.

1. Introduction

Since geophysics corresponds to discontinuities in physical characteristics, it is a non-invasive method of imaging. As computer technology advances, such as data processing and digital transmission, geophysical technologies are evolving quickly. They are successful because they enable rapid and continuous recognition of relatively broad regions instead of the borehole, shaft, or excavation that are examples of local (point) identification (Mita *et al.*, 2018). All common methods used during landslide fieldwork are ground-penetrating radar (GPR) (e.g. Carpentier *et al.*, 2012; Kannaujiya *et al.*, 2019), 2D or 3D seismic methods (e.g. Imani *et al.*, 2021), seismic tomography (e.g. Adamczyk *et al.*, 2013; Stucchi *et al.*, 2014), surface waves surveys [MASW, e.g. Capizzi and Martorana (2014) and Hussain *et al.* (2020)], and electrical resistivity tomography [ERT, e.g. Pasierb *et al.* (2019) and Alpaslan and Bayram (2020)]. Resistivity imaging is currently a widely used technology for landslide investigations due to the sensitivity of electrical resistivity parameter to the mineralogy of the particles, porosity, the groundwater content, the composition of the electrolyte, the conductivity of pore fluid, and clay content (Perrone *et al.*, 2014). This technique provides a quick and light way of gathering spatial information on ground structure, composition (Huntley *et al.*, 2019), determining landslide susceptibility, shear

surface, the geometry of slip plane, depth to bedrock, as well as measuring various sorts of slope deformations in bedrock (Fressard *et al.*, 2016; Ling *et al.*, 2016; Falae *et al.*, 2019; Olabode *et al.*, 2020) and hydrogeology on unstable slopes (Khalil *et al.*, 2018). While less widely employed, 3D resistivity imaging has been utilised to explore the interior structure and hydrogeological regimes associated with landslides (Merritt *et al.*, 2014; Viero *et al.*, 2015). Quick clay, which is common in Scandinavia and North America, is one type of landslide danger for which resistivity imaging has proven to be very useful (Loke *et al.*, 2013). Due to the increased resistivity of rapid (leached) formations in comparison to non-quick (unleached) formations, resistivity imaging has been utilised to find and map formations of the northern regions (Lundström *et al.*, 2009; Solberg *et al.*, 2012; Malehmir *et al.*, 2013; Sauvin *et al.*, 2014). To measure the impacts of saturation, time-lapse resistivity measurements have been done frequently in landslide-prone locations (Friedel *et al.*, 2006; Jomard *et al.*, 2007; Wilkinson *et al.*, 2010; Hayley *et al.*, 2011; Travelletti *et al.*, 2012), and time-lapse resistivity variations have been linked to slope collapse using conceptual models (Piegari *et al.*, 2009). Several recent studies have shown the benefits of using automated resistivity tomography systems with permanent electrode networks to continuously monitor landslide bodies (Meric *et al.*, 2005; Chambers *et al.*, 2013). Using this method, prototype devices have now been deployed to monitor several active landslides (Supper *et al.*, 2014; Jianjun *et al.*, 2020). These approaches are aimed at determining the optimal distribution of electrical resistivity that is compatible with measured values.

Inverse techniques are needed to find the best resistivity distribution that satisfies the experimentally determined apparent resistivity values. Forward modelling is an essential step in geophysical exploration that is used for the calculation of model response during the inversion process. There are several well-known techniques for inverting geoelectrical data. Some algorithms are designed specifically for inverting monitoring (time-lapse) observations or incorporating hydrological or other geophysical data into the inversion process (Blanchy *et al.*, 2020). pyGIMLI (Rücker *et al.*, 2017) and ResIPy (Belanchy *et al.*, 2020), both Python application programming interfaces (API), are successful examples of open-source programs. The latter is a good example of a Graphical User Interface (GUI) that makes the use of complex codes more user-friendly.

The numerical modelling approaches applied to forward modelling of electrical potentials in solving geoelectric problems, used in the former listed research, are finite-difference (FD) and finite-element (FE) approaches. The standard FD approach is simpler to construct and maintain than the FE approach, but it relies on structured rectangular grids. This method implies that local grid refinement is impossible, and any changes in grid size have a significant impact on the total computing resources required. The FE has been developed in recent decades to overcome some of these challenges, and it has the benefit of inherently supporting unstructured meshes. The direct current resistivity (DCR) approach includes modelling and inversion methods created with an unstructured mesh (Ren and Tang, 2010). Additionally, Akça (2016) and Key (2016) use a combination of structured and unstructured meshes to reduce the computational cost of the whole inversion procedure for time-domain induced polarisation (IP) and magnetotelluric (MT), respectively.

Although traditionally, FD mesh consists of rectangular cells that could not readily fit actual topographies, Erdoğan *et al.* (2008) overcame this problem using suitable boundary conditions. Other researchers (e.g. Akça and Basokur, 2010; Thomas and Casten, 2011) also worked on introducing the practice of unstructured mesh for FE and FD forward and inversion calculations to represent complicated structural boundaries by reducing the computation time. Furthermore, Demirci *et al.* (2012) found that if the subterranean structure boundary is not parallel to the surface topography, the borders of these structures may be successfully resolved using inversion utilising the FD forward solution with triangular cells. In summary, structured discretisation of a

physical domain has limitations for correct imaging of intricate geometry of sought target and preserving the variation of rough topography. Therefore, unstructured meshing is imperative for accurate modelling of the physical property and capturing severely rough topography. The unstructured mesh discretization in 2D or 3D studies serves three main purposes, which are: 1) the reduction of model parameters; 2) the capability of constructing any arbitrary topographic relief, and 3) the retrievement of any geometry of sought target (Abedi, 2020).

This work aimed to use synthetic data for comparing the triangular and rectangular mesh-based solutions utilising the ResIPy software to assess the validity of the discovered signals in the field data. To compute the forward model, the open-source code R2 employs a mesh of finite elements. The R2 code implicitly creates simple structured meshes and allows reading externally produced structured/unstructured meshes. This code uses triangular cells with increasing vertical and lateral lengths to create the unstructured mesh. When using structured grid-based methods to produce a mesh with quadrilateral cells, the vertical lengths of the cells increase as the model progresses deeper, but the lateral lengths remain constant.

2. Geoelectrical simulation of a landslide surface

2-D forward modelling, in the inversion process, is employed as an initial model, and it is generally utilised with the FE technique, which has developed as a universal approach for solving differential equations. The inversion procedure ends when the total error is less than 5% or a pre-assigned percentage; otherwise, the error estimate is used to modify model parameters in addition to a damping factor (Jeshvaghani and Darijani, 2014).

As in the real data set of a roto-translational landslide (Fig. 1), a synthetic test case using Schlumberger and Wenner configurations with surface topography was evaluated and compared to demonstrate the validity of the calculative simulation result of a newly developed algorithm

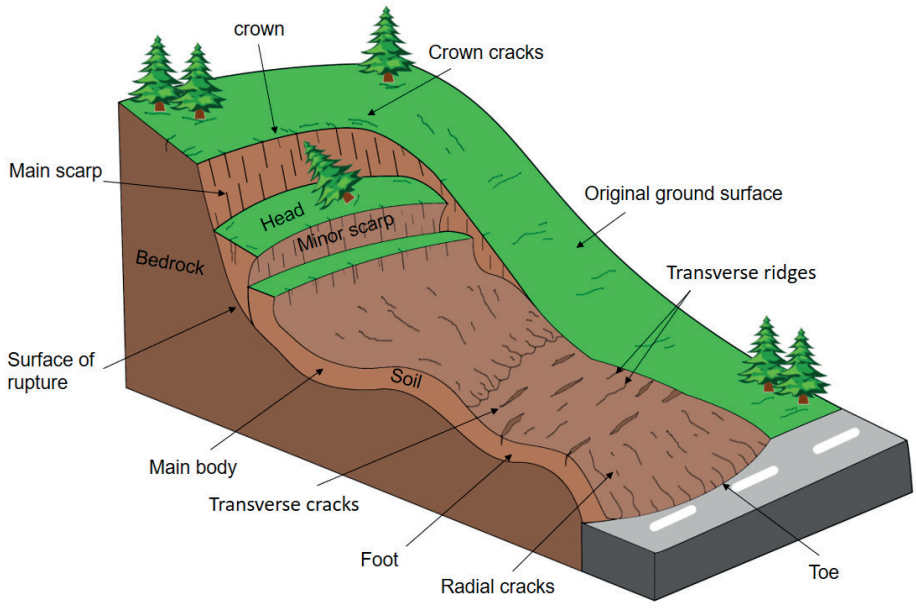

Fig. 1 - A simplified schematic illustration of a landslide surface (Highland and Bobrowsky, 2008).

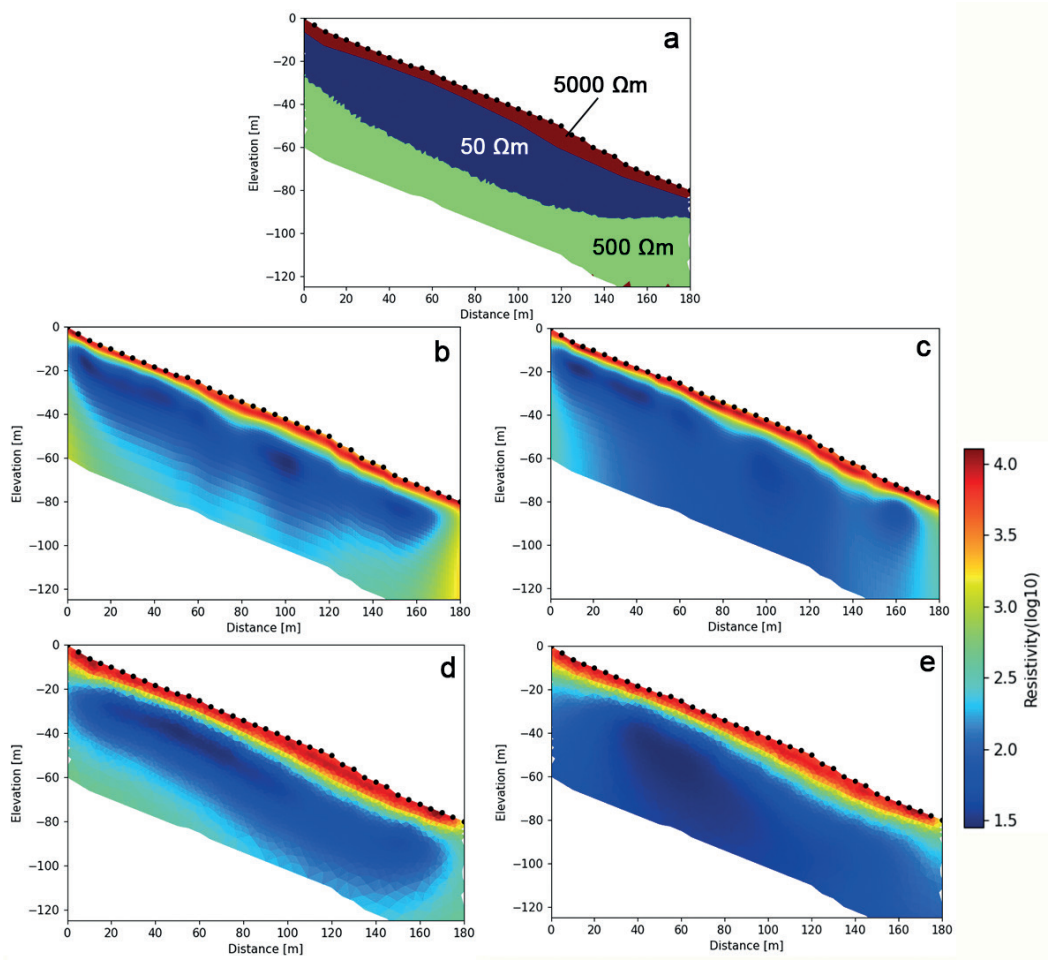

Fig. 2 - The synthetic landslide electrical resistivity model on a rough topography (a); electrical resistivity models after inversion through rectilinear meshing using Schlumberger (b) and Wenner (c) configurations; triangular meshing using Schlumberger (d) and Wenner (e) configurations.

using the GUI of the ResIPy software. The synthetic data are contaminated with 2% Gaussian noise due to the data inaccuracy anticipated for the real data and are then utilised to invert for highlighting the benefits and drawbacks of quadrilateral and triangular meshes in inversion solutions.

Three subregions were created in the synthetic model used to replicate the slip surface structure of the real landslide occurrence near the Tehran-North freeway. Table 1 and Fig. 2a provide three lithological sections underneath the landslide known from field observation and borehole investigation. The model consists of a shallow region immediately under the ground surface filled with cracked rocks such as silt and tuff (5000 Ω·m). While the two deeper regions had more extensive parameters to represent the decline in resolution as the distance from the transmitters and receivers increased. The model comprises coarse-grained carbonate rocks with 500 Ω·m resistivity value, such as marlstone and sandstone basement, and a shale unit with 50 Ω·m resistivity value, which separated the other two units (Fig. 2a). The model is subsequently discretised using both structured and unstructured mesh. Both structured and unstructured grids show a good quality of resistivity models and are not very distant from real values resulting

from the forward solution, which was expected (Fig. 3). The Schlumberger and Wenner arrays are both made up of 37 electrodes spaced 5 m apart. For a constant potential electrode distance, Schlumberger configuration comprises 352 ERT data points; whereas Wenner gave 310 quadrupoles in total. Although Wenner is suitable for characterising horizontal discontinuities and mapping shallow subsurfaces of non-complex landslides, it performs poorly in determining vertical resolution (Figs. 2c and 2e). On the other hand, Schlumberger provides an excellent mapping for the vertical change in resistivity (Figs. 2b and 2d). Moreover, Schlumberger has a higher investigation depth (Figs. 3a, 3c, and 3e) than Wenner configuration (Figs. 3b, 3d, and 3f).

Table 1 - Lithology of subregions for a synthetic test case.

Lithology	Resistivity (Ω·m)
Silt and tuff	5000
Marlstone	500
Shale	50

This section emphasises the speed benefit of an unstructured algorithm over a structured grid-based method. The required time is always significantly reduced since the triangular mesh can represent the model using fewer components in modelling and inversion solutions. In addition to saving time, the inversion takes fewer steps to complete. Table 2 displays the root mean square errors for each inverted model. For both Schlumberger and Wenner configurations, the number of parameters in inversion solutions stated that the unstructured solution took 18 s and 13 s, and the structured solution took 162 s and 94 s, respectively. The borders of the resistivity contrasts are also shown better in the unstructured mesh inversion result than in the structured mesh. We utilised a PC with an Intel Core i5 CPU, 4 GB of RAM, and a 64-bit operating system for all inversion runs.

Table 2 - Synthetic data inversion parameters.

Array Type	Parameters	Structured	Unstructured
Schlumberger	Total time taken	162 s	18 s
	Number of iteration	7	3
	Final RMS Misfit	1.00	1.01
	Total memory required	3.664 Gb	0.118 Gb
Wenner	Total time taken	94 s	13 s
	Number of iteration	6	3
	Final RMS Misfit	1.03	1.01
	Total memory required	3.639 Gb	0.109 Gb

The synthetic model demonstrated that unstructured triangular meshes could handle landslide surface and geological complexity. The use of unstructured meshes has the advantage of substantially decreasing the number of parameters in the solution while keeping the excellent resolution.

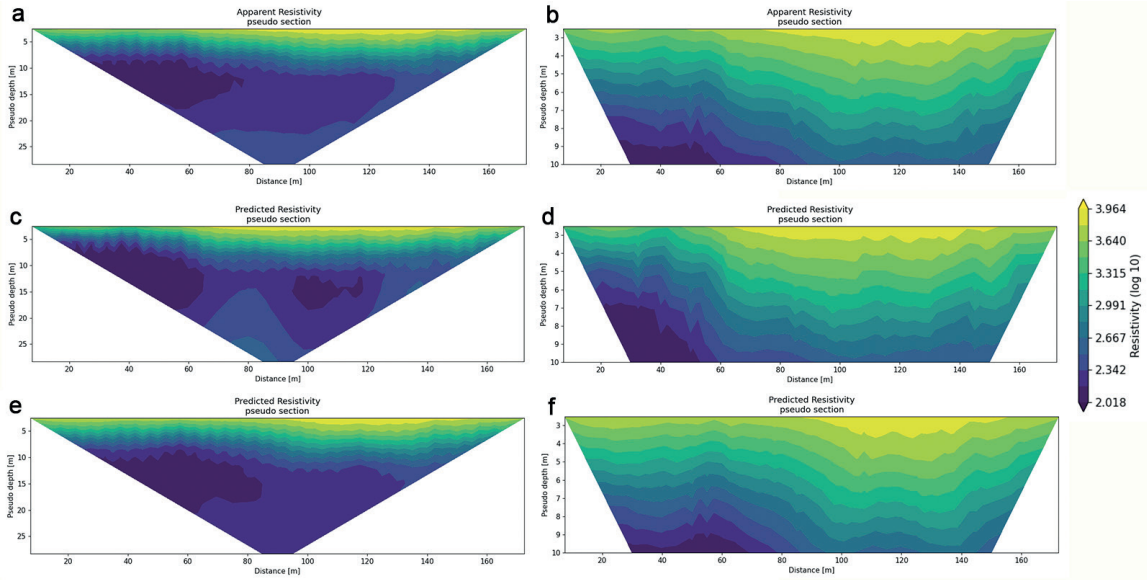

Fig. 3 - Observed apparent resistivity data of the synthetic landslide model of Schlumberger (a) and Wenner (b) configurations; predicted data after inversion through rectilinear meshing of Schlumberger (c) and Wenner (d) configurations; predicted data after inversion through triangular meshing of Schlumberger (e) and Wenner (f) configurations. The topographic effect has been considered in the pseudosections (Fig. 2).

3. Geological descriptions of the landslide area

The data set in this work was obtained from a prone landslide site situated in the southern part of central Alborz falls within the geographical coordinates of latitude 35°58’46” N to 35°58’53” N and longitude 51°16’15” E to 51°16’30” E approximately 20 km to the NW of Tehran, Iran (Fig. 4a). The Tehran-North freeway located between Tehran, Alborz, and the east of Mazandaran provinces has a vital role in terms of transportation and domestic needs. The portion of the study area covered by this study is depicted by the white rectangle as shown in Fig. 4b, which is a landslide hazard zonation map provided by Abedini and Yaghoob Nejad ASL (2017), considering eight main factors in landslide occurrence, including geology, elevation, slope, aspect, distance from the faults, distance from the rivers, land use, and average annual precipitation by conducting the fuzzy model in ArcGIS software. The research area is part of the Tehran map on a scale of 1:100,000 (reproduced from released maps by the Geological Survey of Iran) and is characterised by hilly terrains with surface elevations that vary from 2169 m to 2258 m. The rivers and their distributaries in the area form a dendritic drainage pattern (Fig. 5a).

In a prior study (BZP Consulting Engineers, 2019) on this particular landslide, it was revealed that there are three distinct lithology layers in depths such as alluvium, shale, and weathered marlstone. Based on field observation of the landslide, its surface is largely covered with a layer of coarse-grained alluvium, the constituents of which include tuff mixed with gravels and silt. The alluvium can be up to 10 m thick. The sliding surface of the landslide is shale with tuff alternation and dips 30° with a dip direction of 60° in the southern part of the slide (Fig. 5b). The thickness of the shale is 18 m and is highly fractured. These fractures most likely cause water to penetrate the shale layers and are one of the causes of landslides. In some areas, fractures and joints of shale are observed along with calcite fillings, which can also be seen in field surveys.

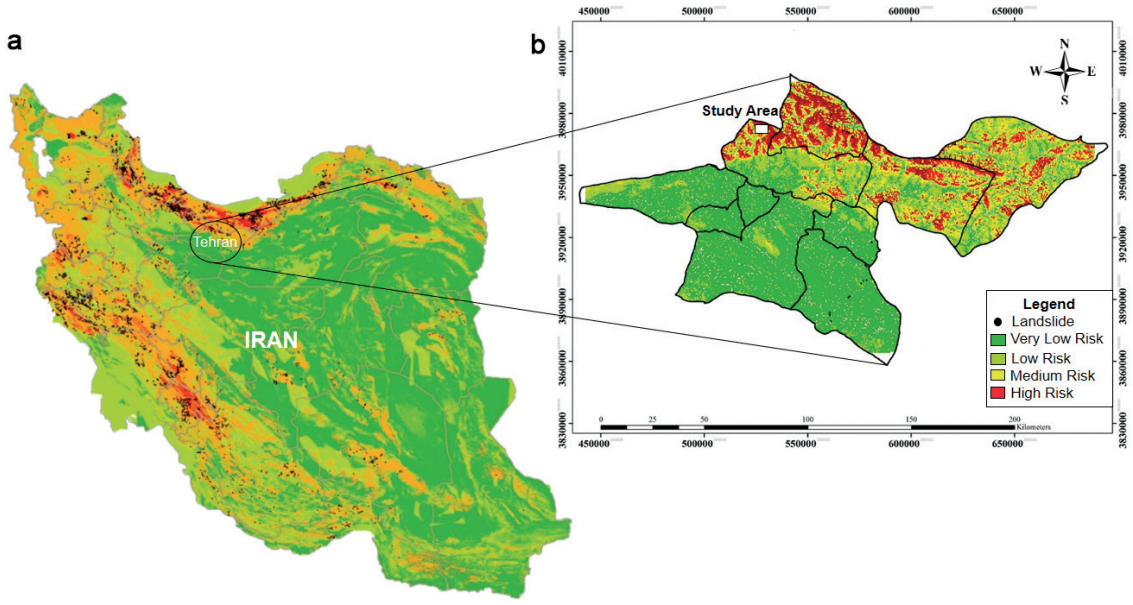

Fig. 4 - Landslide hazard zonation maps: a) Iran published by the Geological Survey of Iran; b) the Tehran province (Abedini and Yaghoob Nejad ASL, 2017), on which the studied area has been shown.

In the northern part of the slide, the hard tuff layers dip 27° with a dip direction of 43° (Fig. 6c). The bedrock in the slide area is weathered marlstone and sand. In addition to the main scarp on the uphill slope, there are a number of minor scarps developed along the radial and transverse cracks. The lithological cross-section of the landslide body along with profile AA' (as shown in Fig. 5c) was drawn on the left flank. All ERT profiles intersect the AA' cross-section.

Borehole investigation and geoelectrical survey have been used in this case to provide the necessary information to delineate the interfaces between the different layers at depths and to identify the likely slip surfaces in the landslide area. Fig. 5b shows the borehole location as well as the profile lines for the ERT survey. According to the borehole investigation data and the inverse image of the geoelectrical Profile (L-7), the landslide characteristics were determined in terms of materials. The borehole encountered three layers, including alluvium, shale, and weathered marlstone up to 15.0 m on depth (Fig. 5d); however, no water table was found up to the drilling depth.

From a tectonic standpoint, the studied region lies between two thrust faults parallel to the Alborz mountain range and are about NW-SE with a 130-150° azimuth, resulting in a series of striking sub-vertical normal faults that extend from NE-SW to N-S. As can be seen in the map (Fig. 5a), the NE-SW fault separates the E_1^{sht} unit from the E_1^{r} and E_1^{tsh} units. The presence of these faults in the vicinity of the studied landslide has crushed and broken rocks and sediments. Moreover, tectonic activities at the fault site have caused the expansion of joints and cracks with the instability of mass movement, allowing water infiltration to accumulate moisture in the underlying levels, hastening the evolution of the instability (Abassi and Yassaghi, 2005). The mentioned landslide area is located in the E_1^{sht} unit, which belongs to the Karaj formation formed in the Eocene period. This landslide is basically a roto-translational form spread over a length of 357 m in total and was initiated due to the road construction process (Fig. 6a). During the field visit, several transverse cracks were observed in the slip crown, which raises the suspicion of extending the sliding range uphill (Fig. 6b). According to drill holes and laboratory geotechnical

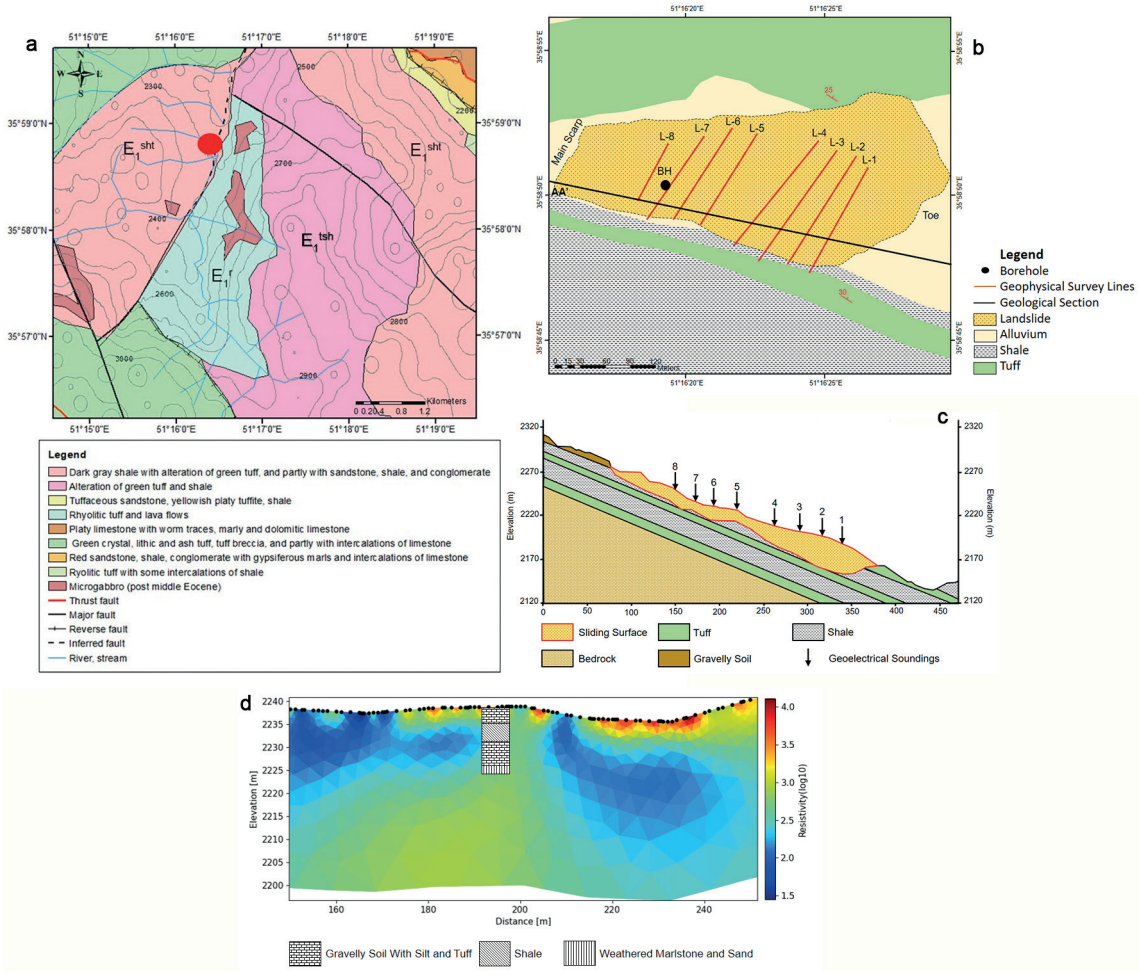

Fig. 5 - Geological map of the studied area (a), the red circle indicates the venue of the studied landslide; geoelectrical profiles and location of the borehole (b); geological cross-section along the landslide body (c); borehole data in complement with inversion interpretation of L-7 profile (d).

analysis of landslide materials, it is further reported that under saturated condition, the shale and tuff are almost cohesionless, and the friction angle is 27°.

4. Methods

4.1. Field data survey

As an active source geophysical method, ERT uses direct current electrodes to determine the distribution of apparent resistivity of a geological medium and image electrical resistivity changes in the electric field with high-resolution variability according to Ohm's law. By taking measurements in various configurations, it is possible to determine the subsurface resistivity depending on the study goal. Traditionally, electrodes are placed in the field along a single line, and the resistivity underneath that line is calculated in two dimensions. A 3D picture may be analysed

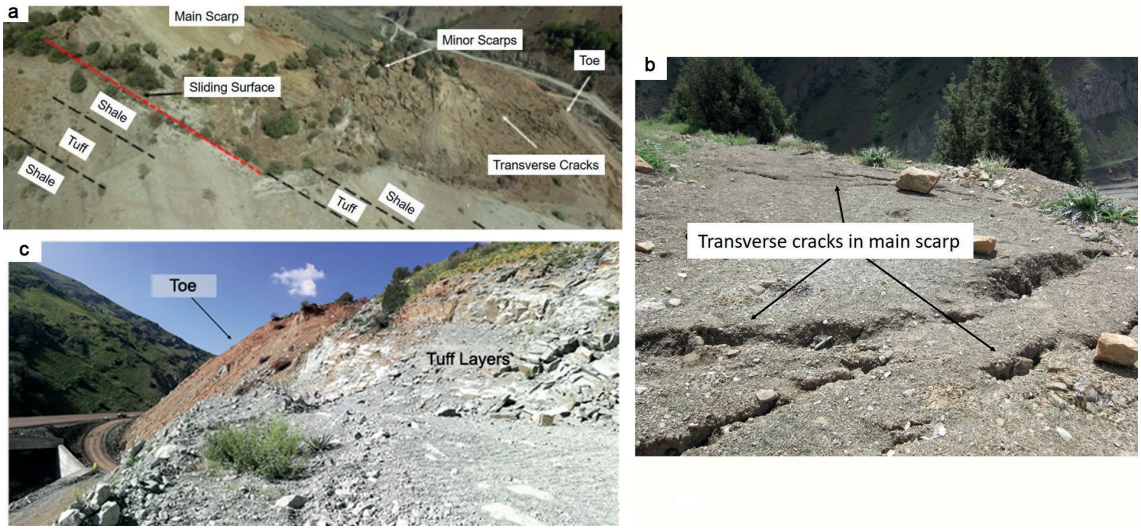

Fig. 6 - Different parts of the landslide (a); evidence of transverse cracks in uphill slope (b); hard tuff layers in the vicinity of the landslide (c) (BZP Consulting Engineers, 2019).

using a 2D array of electrodes on the surface by inverting all the acquired data. This is possible if the distance between the parallel profiles is not greater than the investigation depth. Different electrode configurations (quadrupole geometry) are feasible. The ERT method combines Vertical Electrical Sounding (VES) (deeper penetration) and electrical profiling (measurements along with the profile). The parameters of the medium, such as humidity, porosity, and salinity, impact the depth of penetration (Loke, 2015). It is feasible to apply 2D interpretation since the ERT approach has a better spatial resolution. Advanced computational approaches assist in reducing ambiguity in solutions and creating a 2D image of the apparent resistivity distribution that is as similar to the true resistivity distribution as possible. However, more complex structures can only be adequately represented by a 3D subsurface model (Barker and Loke, 1996). In this work, using the Schlumberger setup and the WDDS-1 (BTSK) measuring device, field measurements were taken with eight parallel lines ranging in length from 60 to 130 m, directly on the surface with an E-W trend and spaced roughly 20 m apart (except for profiles 4 and 5) resulted in 58 electrodes in total. The data are, then, analysed using ERT inversion software ResIPy developed by Blanchy *et al*. (2020) to create a resistivity model that depicts the research region in 2D. Since the issue has a non-linear nature, the inversion process is repeated until the misfit between the expected result and the measured response is within a certain tolerance. This misfit must be minimised. The slope and depth of the sliding surface area of the probable landslide region are calculated using resistivity data.

4.2. Inversion

In this study, we give the inversion findings of the gathered data in four field data profiles (2, 4, 6, 8) that may be compared to the lithology of the area based on borehole data and field observations. From illustrations of apparent (Figs. 7a, 9a, 11a, 13a) and predicted resistivity data obtained from both structured (Figs. 7b, 9b, 11b, 13b) and unstructured (Figs. 7c, 9c, 11c, 13c) mesh-based inversion solutions, it can be concluded that both methods show a good misfit between real and calculated data using each algorithm. However, the information provided

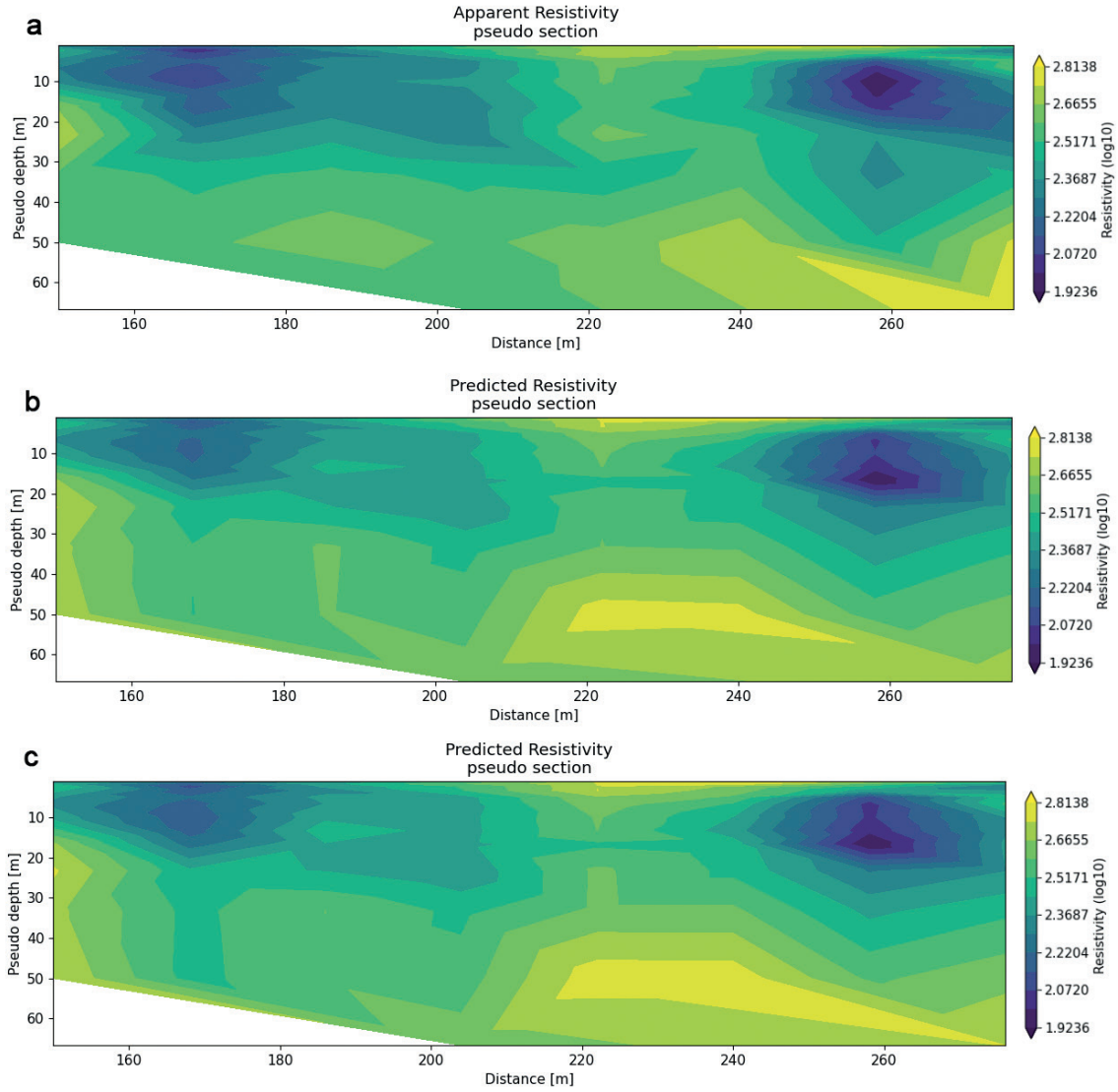

Fig. 7 - Observed apparent resistivity data along profile 2 (a); predicted data after inversion through rectilinear meshing (b); and triangular meshing (c).

Table 3 - Information gained from real data inversion.

	Mesh	Total time taken (s)	Final RMS Misfit (%)
Line 2	Structured	2942	1.29
	Unstructured	312	1.16
Line 4	Structured	2850	1.00
	Unstructured	85	1.00
Line 6	Structured	1192	1.01
	Unstructured	39	1.02
Line 8	Structured	289	0.99
	Unstructured	5	1.00

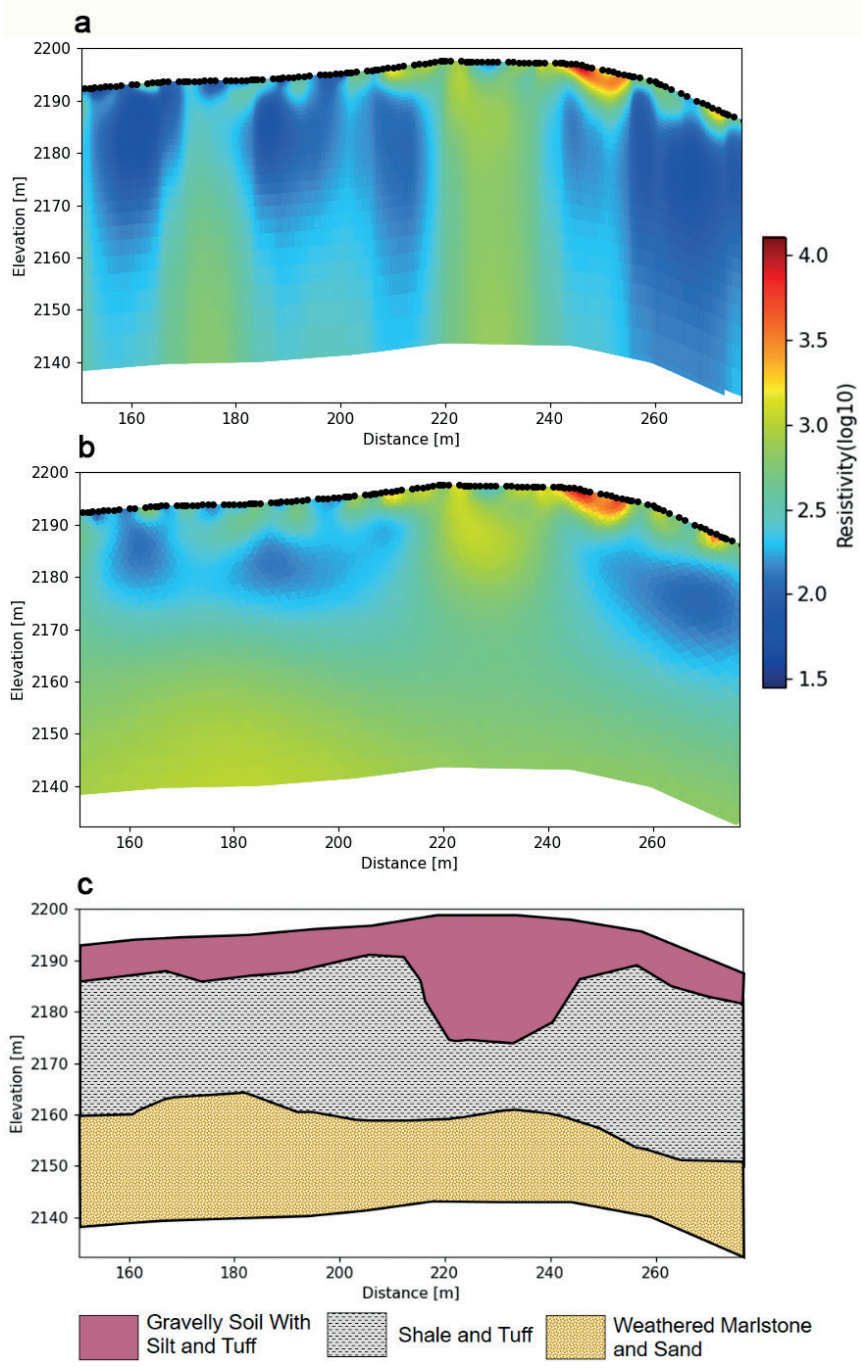

Fig. 8 - Electrical resistivity models along profile 2 after inversion through rectilinear meshing (a); triangular meshing (b); and geological model inferred from electrical images (c).

comparatively from the results in Table 3 confirms the fact that using a triangular mesh-based algorithm requires less time to gain an acceptable result.

The structured (Figs. 8a, 10a, 12a, and 14a) and unstructured (Figs. 8b, 10b, 12b, and 14b) mesh-based algorithms were used to invert the obtained data separately. The

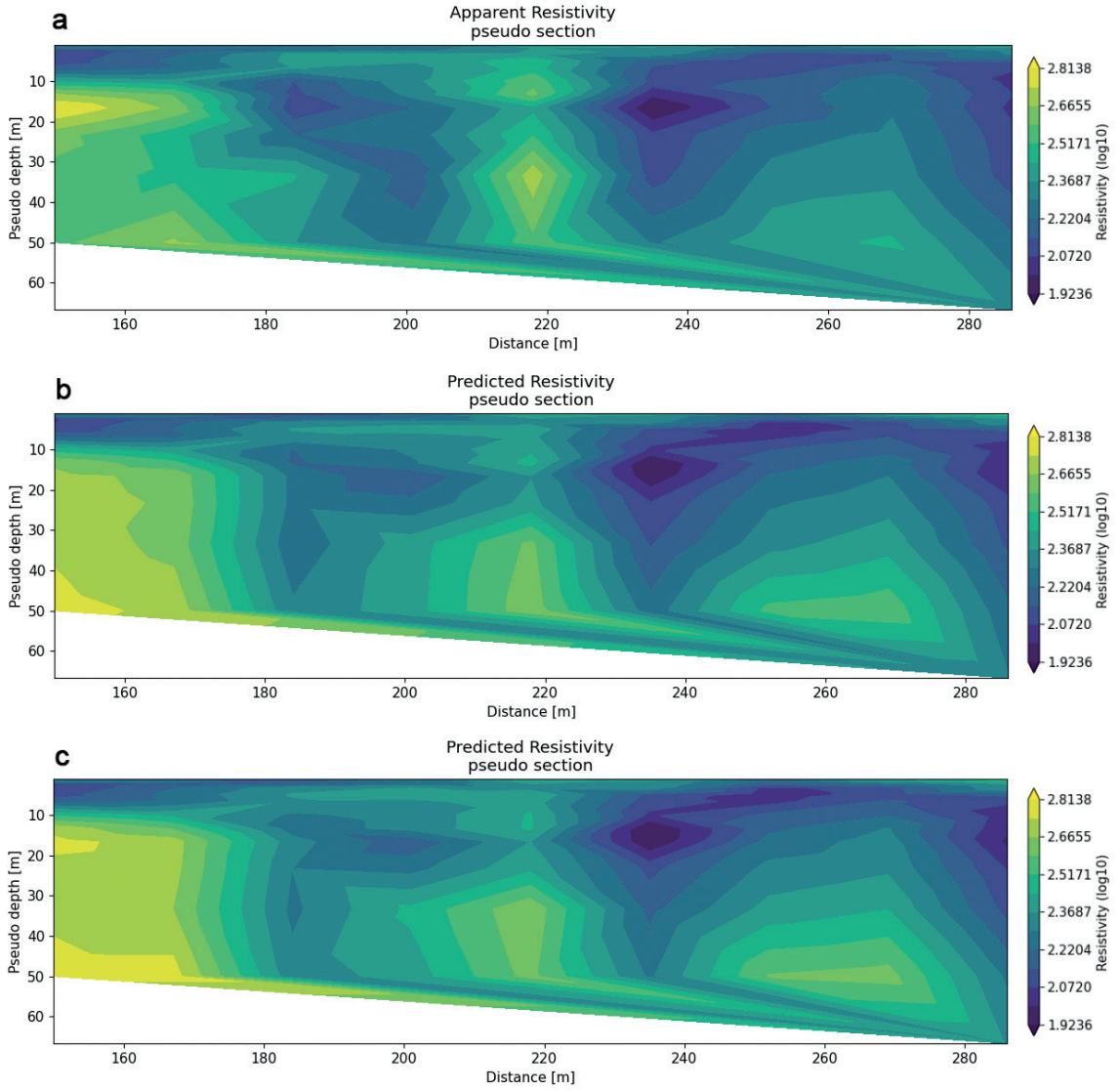

Fig. 9 - Observed apparent resistivity data along profile 4 (a); predicted data after inversion through rectilinear meshing (b); and triangular meshing (c).

lithology determined from resistivity distribution models is represented in Figs. 8c, 10c, 12c, and 14c.

The unstructured inversion is more successful in differentiating both conductive and resistive structures than the structured method. The new technique uses an unstructured mesh to find the boundaries of shale, marlstone, and tuff. The fact that the findings of the unstructured inversion match the data acquired from field observation and borehole demonstrates the benefit and effectiveness of the unstructured mesh inversion.

For all the profiles, the sliding surface with around a 20-m thickness was located at the transition zone with low resistivity ($\rho \leq 500\ \Omega{\cdot}m$) between the sliding material and the bedrock with high resistivity ($\rho \geq 500\ \Omega{\cdot}m$). Alluvium with a wide range of resistivity is encountered up to a depth of about 10 m. At the sides of the resistivity section beyond 10-m depth, the bedrock

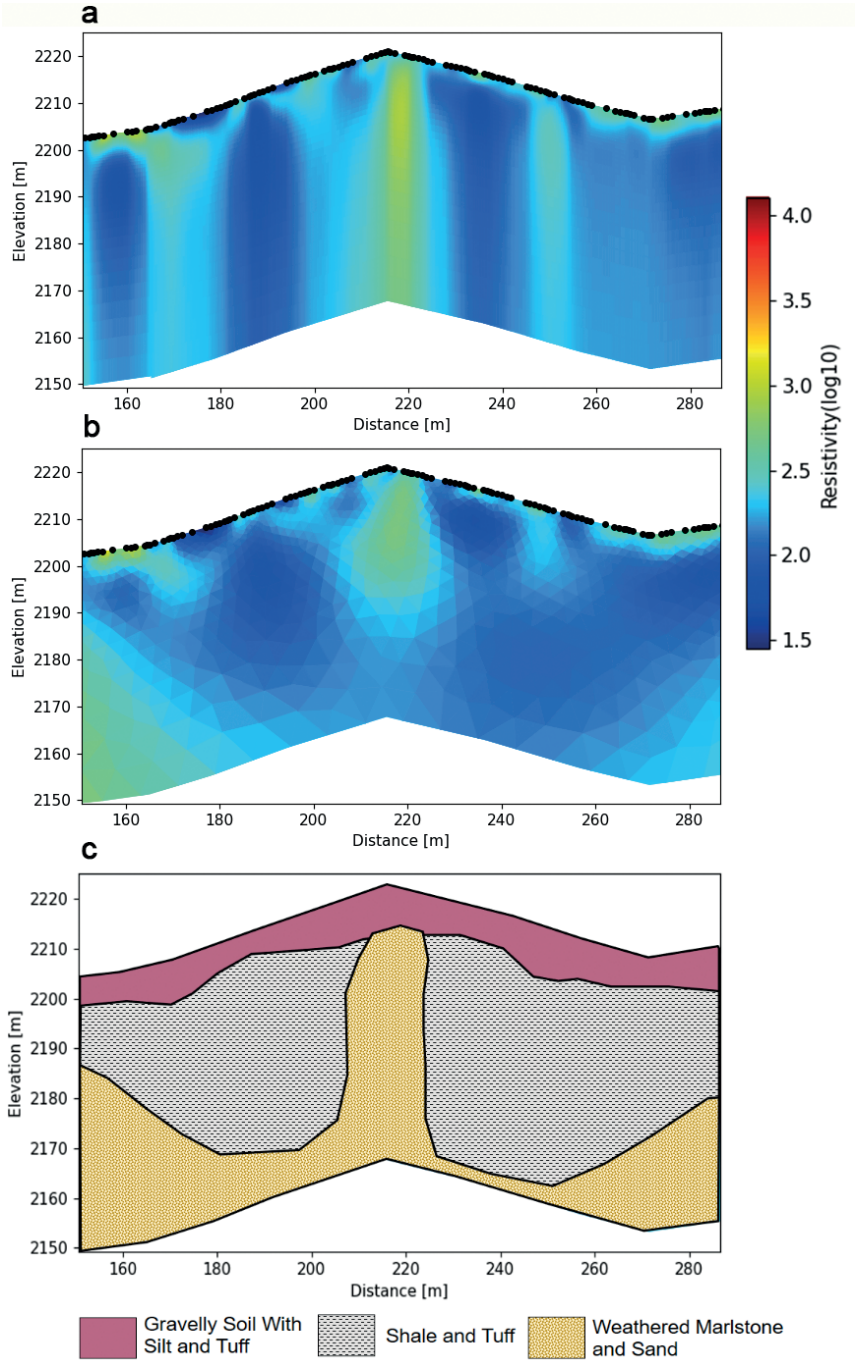

Fig. 10 - Electrical resistivity models along profile 4 after inversion through rectilinear meshing (a); triangular meshing (b); and geological model inferred from electrical images (c).

consists of weathered marlstone, and sand is reached till the total depth of penetration (i.e. 58 m). The landslide slip surface is thought to be at the intersection of weathered marlstone and alluvium layers. Fig. 15a depicts the 2D inverted cross-sections in a 3D view. From this illustration and Fig. 15b, it is evident that the area suffered from an undulated topography, and the possibility

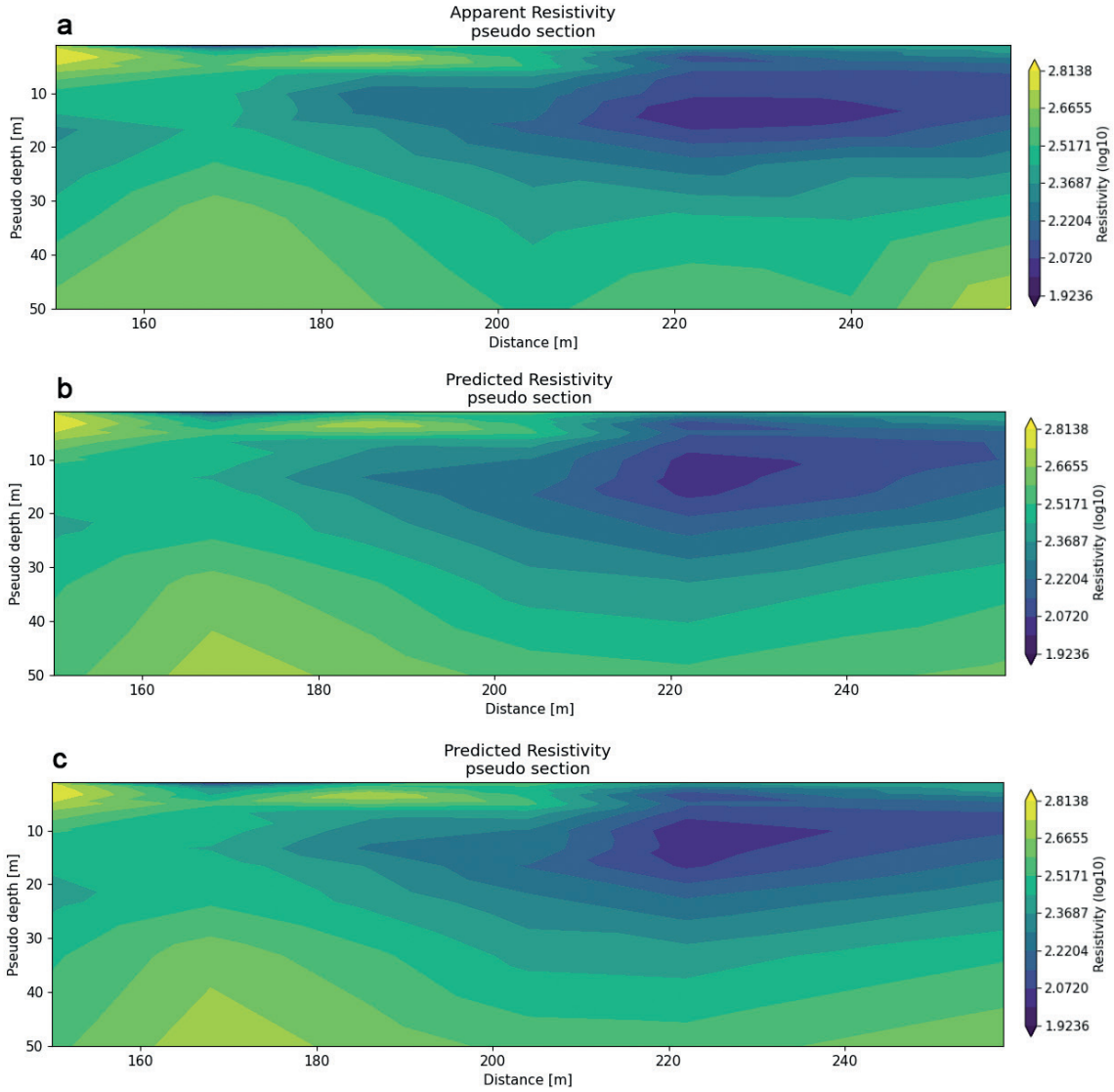

Fig. 11 - Observed apparent resistivity data along profile 6 (a); predicted data after inversion through rectilinear meshing (b); and triangular meshing (c).

of prone landslide occurrence in the region is high due to the existence of shale units in the area. Prone landslide can be activated after a rainstorm in particular seasons.

5. Discussion and conclusion

In some circumstances, forward modelling is required to explain the structures that emerge on resistivity models. Geophysical interpretation can be incorrect or even misleading without this technique. The Tehran-North freeway landslide event permitted testing the reliability of the generated resistivity model. For forward modelling, the Finite Element Method (FEM) was applied. It is commonly known that the FEM modelling algorithms are slower, however, more

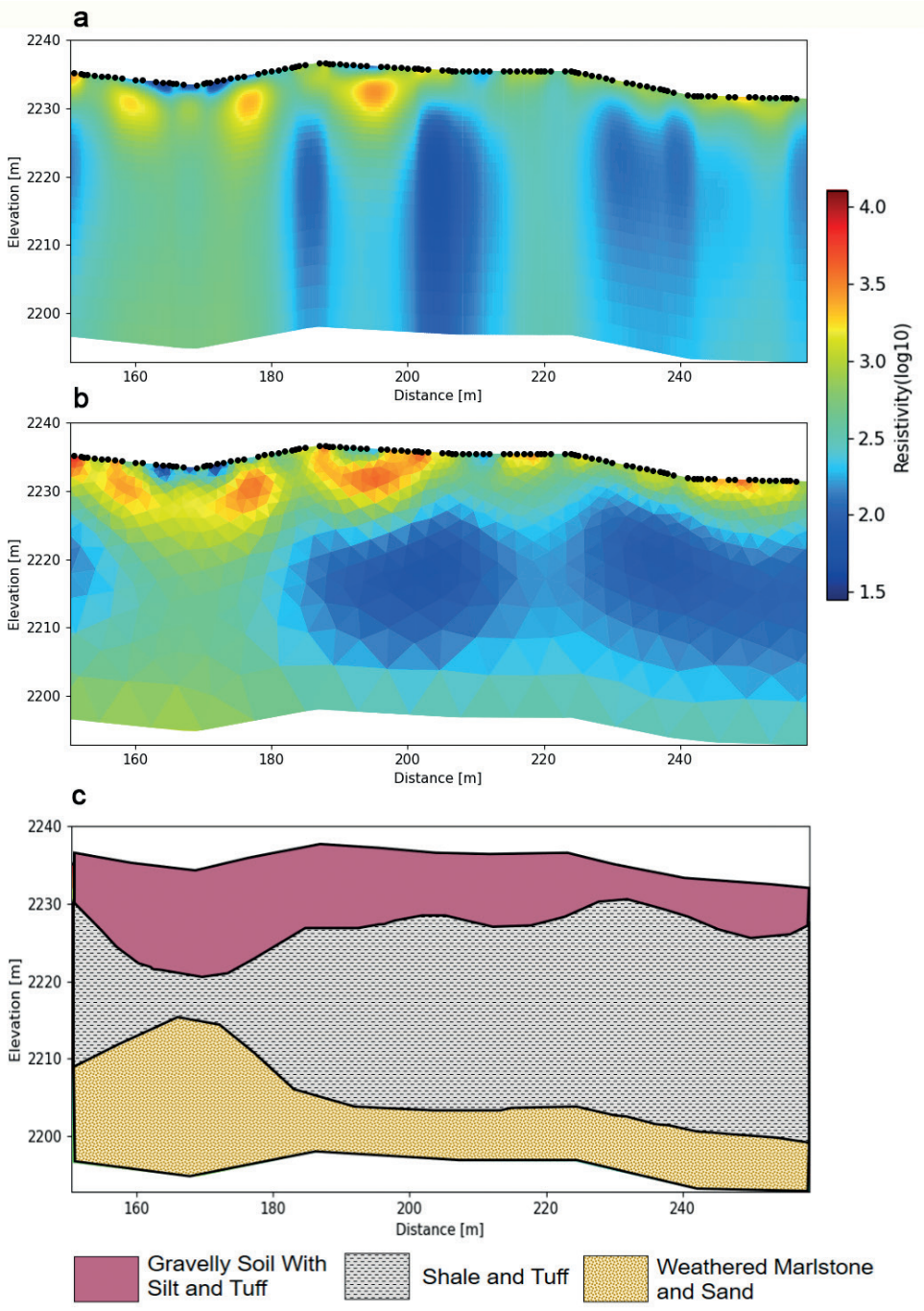

Fig. 12 - Electrical resistivity models along profile 6 after inversion through rectilinear meshing (a); triangular meshing (b); and geological model inferred from electrical images (c).

exact than the Finite Difference Method (FDM). This problem of the FEM is overcome with regard to the unstructured mesh, allowing the method to conduct both speedy and exact modelling. The performance of both rectangular and triangular algorithms for 2D inversion was examined using synthetic and field data from the geoelectrical survey with rugged topography.

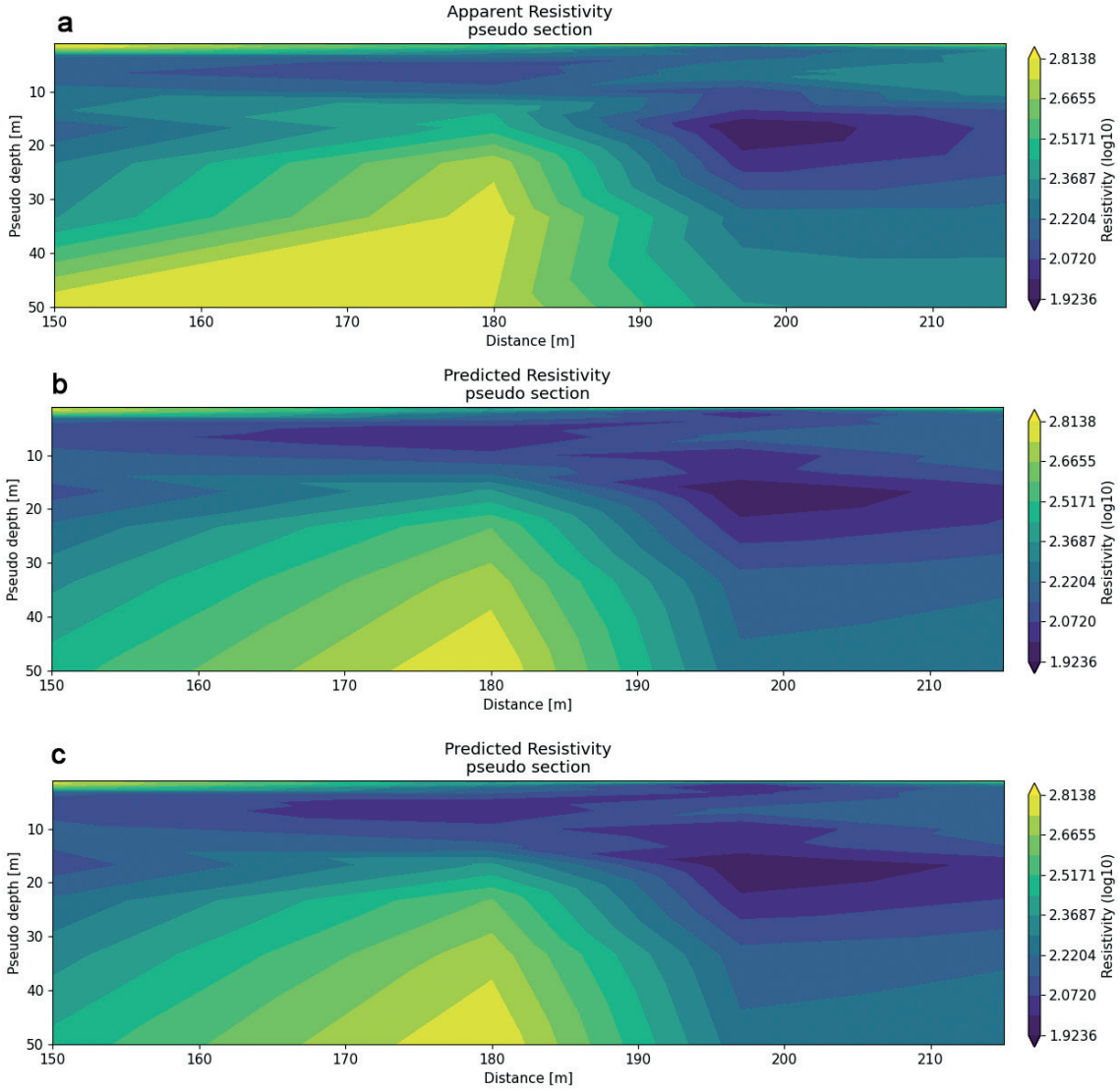

Fig. 13 - Observed apparent resistivity data along profile 8 (a); predicted data after inversion through rectilinear meshing (b); and triangular meshing (c).

According to the interpretation of field observations and drill investigations, the synthetic landslide body consists of three-layered strata (Table 1 and Fig. 2a). The first layer is considered to have a greater resistivity of 5000 Ω·m, which corresponds to alluvium. The second layer has a low resistivity value of 50 Ω·m and can be interpreted as shale. The third layer, which is weathered marlstone, has a high resistivity value of 500 Ω·m. The results of an unstructured grid-based method are compared to a structured FEM numerical solution. Unstructured algorithms require fewer components than structured grid algorithms for imaging surface topography and subterranean resistivity structures. We also discovered that the mesh quality improves when unstructured grids are employed, and numerical errors decrease dramatically. As a result, the software is faster and more reliable than traditional inversion techniques for simulating complicated surface topography. According to our synthetic data examination, the resistivity

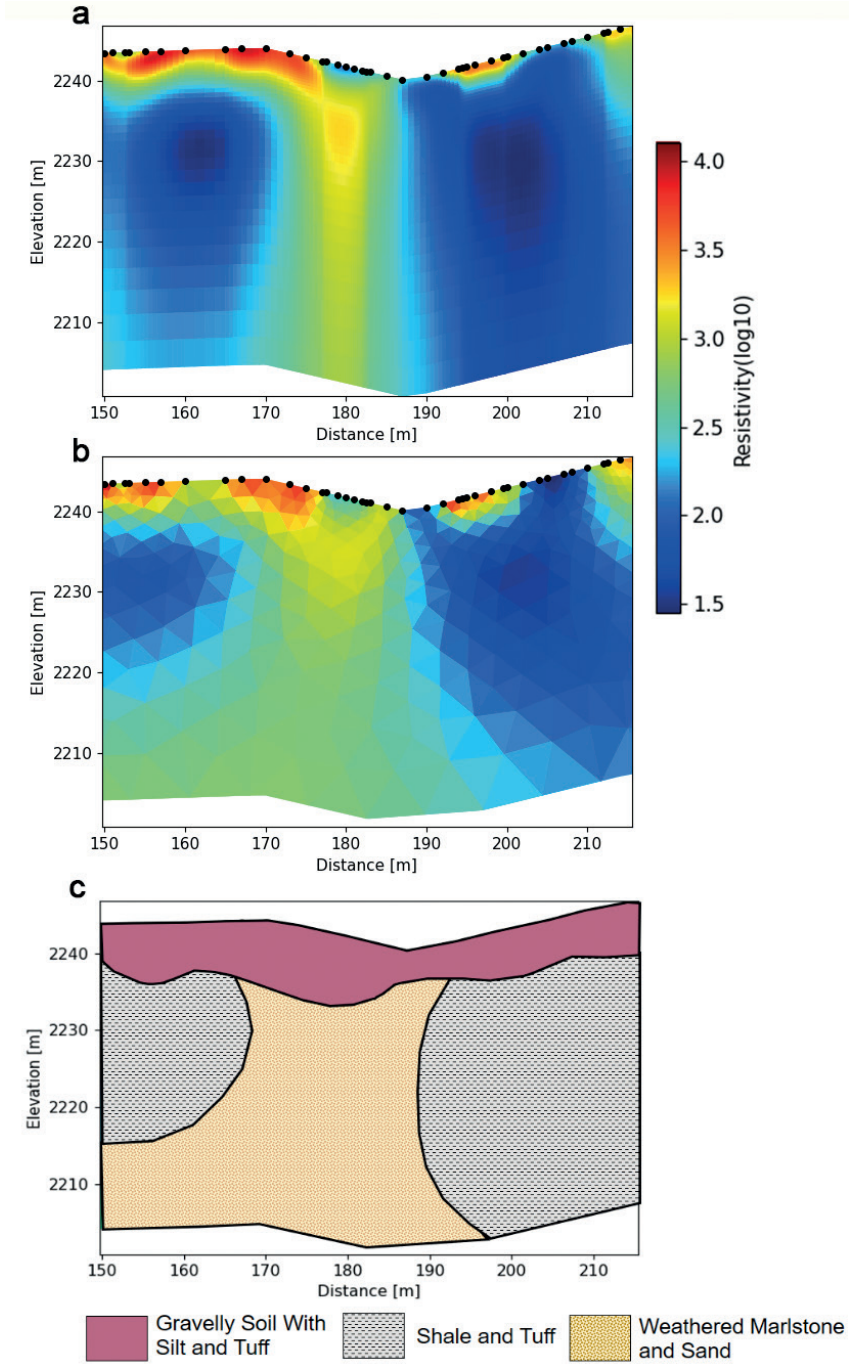

Fig. 14 - Electrical resistivity models along profile 8 after inversion through rectilinear meshing (a); triangular meshing (b); and geological model inferred from electrical images (c).

values and bounds produced from the structured and unstructured mesh-based procedures are close enough to those of the synthetic model. However, synthetic and field data results confirm the speed and accuracy superiority of the unstructured approach over traditional structured grid-based inversion techniques.

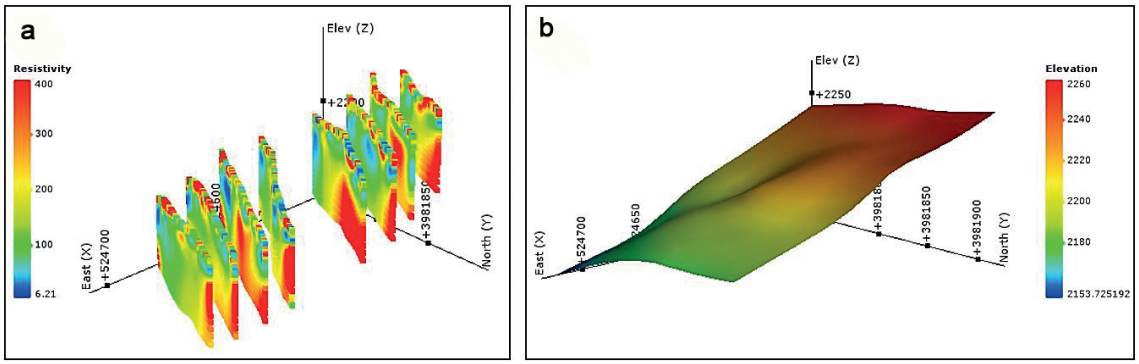

Fig. 15 - 3D visualisation of all inverted 2D models (a) and a schematic map of the landslide surface (b).

The non-invasive geoelectrical approach was demonstrated to be suitable for landslide investigation in association with drilling investigation, enabling the delineating of the slip surface. As a result, its use is highly recommended for monitoring landslides to provide early risk warnings in order to avoid damage to buildings or human life.

Acknowledgments. The authors acknowledge the help received from the Mining Engineering School, University of Tehran. We also like to thank Bonyan Zamin Paydar Consulting Engineers for providing the data.

REFERENCES

Abassi A.R. and Yassaghi A.; 2005: *Geometry and kinematic analysis of Laniz structural sub-zone; evidence for structural evolution of south central Alborz.* Geosci., 56, 152-167, in Persian.

Abedi M.; 2020: *A focused and constrained 2D inversion of potential feld geophysical data through Delaunay triangulation, a case study for iron-bearing targeting at the Shavaz deposit in Iran.* Phys. Earth Planet. Inter., 309, 106604, doi:10.1016/j.pepi.2020.106604.

Abedini M. and Yaghoob Nejad ASL N.; 2017: *Risk zonation of the landslides in Tehran province using Fuzzy model.* J. Emergency Manage., 6, 145-155.

Adamczyk A., Malinowski M. and Malehmir A.; 2013: *Application of first-arrival tomography to characterize a quick clay landslide site in southwest Sweden.* Acta Geophys., 61, 1057-1073, doi: 10.2478/s11600-013-0136-y.

Akça I.; 2016: *ELRIS2D: a MATLAB package for the 2D inversion of DC resistivity/IP data.* Acta Geophys., 64, 443-462, doi: 10.1515/acgeo-2015-0071.

Akça I. and Basokur A.T.; 2010: *Extraction of structure-based geoelectric models by hybrid genetic algorithms.* Geophys., 75, F15-F22, doi: 10.1190/1.3273851.

Alpaslan N. and Bayram M.; 2020: *Landslide study with 2D electrical resistivity tomography (ERT): a case study from Turkey.* Carpathian J. Earth Environ. Sci., 15, 391-403, doi: 10.26471/CJEES/2020/015/139.

Barker R.D. and Loke M.H.; 1996: *Practical techniques for 3D resistivity surveys and data inversion.* Geophys. Prospect., 44, 499-523, doi: 10.1111/j.1365-2478.1996.tb00162.x.

Blanchy G., Saneiyan S., Boyd J., McLachlan P. and Binley A.; 2020: *ResIPy, an intuitive open source software for complex geoelectrical inversion/modelling.* Comput. Geosci., 137, 1-12, doi: 10.1016/j.cageo.2020.104423.

BZP Consult Engineers; 2019: *Geology, engineering geology, stability analysis and presentation of landslide trench safety solutions in the area of 28 km of Tehran-North freeway area 1*. Tecnical Report.

Capizzi P. and Martorana R.; 2014: *Integration of constrained electrical and seismic tomographies to study the landslide affecting the cathedral of Agrigento.* J. Geophys. Eng., 11, 045009, doi: 10.1088/1742-2132/11/4/045009.

Carpentier S., Konz M., Fischer R., Anagnostopoulos G., Meusburger K. and Schoeck K.; 2012: *Geophysical imaging of shallow subsurface topography and its implication for shallow landslide susceptibility in the Urseren Valley, Switzerland.* J. Appl. Geophys., 83, 46-56, doi: 10.1016/j.jappgeo.2012.05.001.

Chambers J., Meldrum P., Gunn D., Wilkinson P., Merritt A., Murphy W., West J., Kuras O., Haslam E., Hobbs P., Pennington C. and Munro C.; 2013: *Geophysical-geotechnical sensor networks for landslide monitoring.* In: Margottini C. (ed), Landslide Science and Practice, Springer, Berlin, Germany, Vol. 2, pp. 289-294, doi: 10.1007/978-3-642-31445-2_37.

Demirci I., Erdoğan E. and Candansayar M.E.; 2012: *Two-dimensional inversion of direct current resistivity data incorporating topography by using finite difference techniques with triangle cells: investigation of Kera fault zone in western Crete.* Geophys., 77, E67-E75, doi: 10.1190/geo2011-0130.1.

Erdoğan E., Demirci I. and Candansayar M.E.; 2008: *Incorporating topography into 2D resistivity modelling using finite-element and finite-difference approaches*. Geophys., 73, F135-F142, doi: 10.1190/1.2905835.

Falae P.O., Kanungo D.P., Chauhan P.K.S. and Dash R.K.; 2019: *Electrical resistivity tomography (ERT) based subsurface characterisation of Pakhi landslide, Garhwal Himalayas, India.* Environ. Earth Sci., 78, 1-18, doi: 10.1007/s12665-019-8430-x.

Fressard M., Maquaire O., Thiery Y., Davidson R. and Lissak C.; 2016: *Multi-method characterisation of an active landslide: case study in the Pays d'Auge plateau (Normandy, France).* Geomorphol., 270, 22-39, doi: 10.1016/j.geomorph.2016.07.001.

Friedel S., Thielen A. and Springman S.M.; 2006: *Investigation of a slope endangered by rainfall-induced landslides using 3D resistivity tomography and geotechnical testing.* J. Appl. Geophys., 60, 100-114, doi: 10.1016/j.jappgeo.2006.01.001.

Hayley K., Pidlisecky A. and Bentley L.R.; 2011: *Simultaneous time-lapse electrical resistivity inversion.* J. Appl. Geophys., 75, 401-411, doi: 10.1016/j.jappgeo.2011.06.035.

Highland L.M. and Bobrowsky P.; 2008: *The landslide handbook - A guide to understanding landslides.* U.S. Geological Survey, Reston, VA, USA, Circ. 1325, 147 pp., doi: 10.3133/cir1325.

Huntley D., Bobrowsky P., Hendry M., Macciotta R. and Best M.; 2019: *Application of multi-dimensional electrical resistivity tomography datasets to investigate a very slow-moving landslide near Ashcroft, British Columbia, Canada*. Landslides, 16, 1033-1042, doi: 10.1007/s10346-019-01147-1.

Hussain Y., Hamza O., Cárdenas-Soto M., Borges W.R., Dou J., Rebolledo J.F.R. and Prado R.L.; 2020: *Characterization of Sobradinho landslide in fluvial valley using masw and ert methods.* REM - Int. Eng. J., 73, 487-497, doi: 10.1590/0370-44672019730109.

Imani P., Tian G., Hadiloo S. and El-Raouf A.A.; 2021: *Application of combined electrical resistivity tomography (ERT) and seismic refraction tomography (SRT) methods to investigate Xiaoshan district landslide site: Hangzhou, China.* J. Appl. Geophys., 184, 104236, doi: 10.1016/j.jappgeo.2020.104236.

Jeshvaghani M.S. and Darijani M.; 2014: *Two-dimensional geomagnetic forward modelling using adaptive finite element method and investigation of the topographic effect.* J. Appl. Geophys., 105, 169-179, doi: 10.1016/j.jappgeo.2014.03.016.

Jianjun G., Zhang Y.X. and Xiao L.; 2020: *An application of the high-density electrical resistivity method for detecting slide zones in deep-seated landslides in limestone areas.* J. Appl. Geophys., 177, 104013, doi: 10.1016/j.jappgeo.2020.104013.

Jomard H., Lebourg T. and Tric E.; 2007: *Identification of the gravitational boundary in weathered gneiss by geophysical survey: La Clapière landslide (France).* J. Appl. Geophys., 62, 47-57, doi: 10.1016/j.jappgeo.2006.07.003.

Kannaujiya S., Chattoraj S.L., Jayalath D., Ray P.K.C., Bajaj K., Podali S. and Bisht M.P.S.; 2019: *Integration of satellite remote sensing and geophysical techniques (electrical resistivity tomography and ground penetrating radar) for landslide characterization at Kunjethi (Kalimath), Garhwal Himalaya, India*. Nat. Hazards, 97, 1191-1208, doi: 10.1007/s11069-019-03695-0.

Key K.; 2016: *MARE2DEM: a 2-D inversion code for controlled-source electromagnetic and magnetotelluric data.* Geophys. J. Int., 207, 571-588, doi: 10.1093/gji/ggw290.

Khalil M.A., Bobst A. and Mosolf J.; 2018: *Utilizing 2D electrical resistivity tomography and very low frequency electromagnetics to investigate the hydrogeology of natural cold springs near Virginia city, southwest Montana.* Pure Appl. Geophys., 175, 3525-3538, doi: 10.1007/s00024-018-1865-2.

Ling C., Xu Q., Zhang Q., Ran J. and Lv H.; 2016: *Application of electrical resistivity tomography for investigating the internal structure of a translational landslide and characterizing its groundwater circulation (Kualiangzi landslide, southwest China).* J. Appl. Geophys., 131, 154-162, doi: 10.1016/j.jappgeo.2016.06.003.

Loke M.H.; 2015: *Tutorial: 2D and 3D electrical imaging surveys.*

Loke M.H, Chambers J.E., Rucker D.F., Kuras O. and Wilkinson P.B.; 2013: *Recent developments in the direct-current geoelectrical imaging method.* J. Appl. Geophys., 95, 135-156, doi: 10.1016/j.jappgeo.2013.02.017.

Lundström K., Larsson R. and Dahlin T.; 2009: *Mapping of quick clay formations using geotechnical and geophysical methods.* Landslides, 6, 1-15, doi: 10.1007/s10346-009-0144-9.

Malehmir A., Bastani M., Krawczyk C.M., Gurk M., Ismail N., Polom U. and Persson L.; 2013: *Geophysical assessment and geotechnical investigation of quick-clay landslides - A Swedish case study*. Near Surf. Geophys., 11, 341-350, doi: 10.3997/1873-0604.2013010.

Meric O., Garambois S., Jongmans D., Wathelet M., Chatelain J.L. and Vengeon J.M.; 2005: *Application of geophysical methods for the investigation of the large gravitational mass movement of Séchilienne, France.* Can. Geotech. J., 42, 1105-1115, doi: 10.1139/t05-034.

Merritt A.J., Chambers J.E., Murphy W., Wilkinson P.B., West L.J., Gunn D.A., Meldrum P.I., Kirkham M. and Dixon N.; 2014: *3D ground model development for an active landslide in Lias mudrocks using geophysical, remote sensing and geotechnical methods.* Landslides, 11, 537-550, doi: 10.1007/s10346-013-0409-1.

Mita M., Glazer M., Kaczmarzyk R., Dąbrowski M. and Mita K.; 2018: *Case study of electrical resistivity tomography measurements used in landslides investigation, southern Poland.* Contemp. Trends. Geosci., 7, 110-126, doi: 10.2478/ctg-2018-0007.

Olabode O.P., San L.H. and Ramli M.H.; 2020: *Analysis of geotechnical-assisted 2-D electrical resistivity tomography monitoring of slope instability in residual soil of weathered granitic basement.* Front. Earth Sci., 8, 1-15, doi: 10.3389/feart.2020.580230.

Pasierb B., Grodecki M. and Gwóźdź R.; 2019: *Geophysical and geotechnical approach to a landslide stability assessment: a case study.* Acta Geophys., 67, 1823-1834, doi: 10.1007/s11600-019-00338-7.

Perrone A., Lapenna V. and Piscitelli S.; 2014: *Electrical resistivity tomography technique for landslide investigation: a review*. Earth Sci. Rev., 135, 65-82, doi: 10.1016/j.earscirev.2014.04.002.

Piegari E., Cataudella V., Di Maio R., Milano L., Nicodemi M. and Soldovieri M.G.; 2009: *Electrical resistivity tomography and statistical analysis in landslide modelling: a conceptual approach.* J. Appl. Geophys., 68, 151-158, doi: 10.1016/j.jappgeo.2008.10.014.

Ren Z. and Tang J.; 2010: *3D direct current resistivity modelling with unstructured mesh by adaptive finite-element method.* Geophys., 75, 6-17, doi: 10.1190/1.3298690.

Rücker C., Günther T. and Wagner F.M.; 2017: *pyGIMLi: an open-source library for modelling and inversion in geophysics.* Comput. Geosci., 109, 106-123, doi: 10.1016/j.cageo.2017.07.011.

Sauvin G., Lecomte I., Bazin S., Hansen L., Vanneste M. and L'Heureux J.S.; 2014: *On the integrated use of geophysics for quick-clay mapping: the Hvittingfoss case study, Norway.* J. Appl. Geophys., 106, 1-13, doi: 10.1016/j.jappgeo.2014.04.001.

Solberg I.L., Hansen L., Rønning J.S., Haugen E.D., Dalsegg E. and Tønnesen J.F.; 2012: *Combined geophysical and geotechnical approach to ground investigations and hazard zonation of a quick clay area, mid Norway*. Bull. Eng. Geol. Environ., 71, 119-133, doi: 10.1007/s10064-011-0363-x.

Stucchi E., Ribolini A. and Anfuso A.; 2014: *High-resolution reflection seismic survey at the Patigno landslide, northern Apennines, Italy.* Near Surf. Geophys., 12, 559-571, doi: 10.3997/1873-0604.2013036.

Supper R., Ottowitz D., Jochum B., Kim J.H., Romer A., Baro I., Pfeiler S., Lovisolo M., Gruber S. and Vecchiotti F.; 2014: *Geoelectrical monitoring: an innovative method to supplement landslide surveillance and early warning.* Near Surf. Geophys., 12, 133-150, doi: 10.3997/1873-0604.2013060.

Thomas G. and Carsten R.; 2011: *Boundless Electrical Resistivity Tomography BERT - The user tutorial, v. 1.0.* Interface, 28 pp.

Travelletti J., Sailhac P., Malet J.P., Grandjean G. and Ponton J.; 2012: *Hydrological response of weathered clay-shale slopes: water infiltration monitoring with time-lapse electrical resistivity tomography.* Hydrol. Processes, 26, 2106-2119, doi: 10.1002/hyp.7983.

Viero A., Galgaro A., Morelli G., Breda A. and Francese R.G.; 2015: *Investigations on the structural setting of a landslide-prone slope by means of three-dimensional electrical resistivity tomography.* Nat. Hazards, 78, 1369-1385, doi: 10.1007/s11069-015-1777-8.

Wilkinson P.B., Chambers J.E., Meldrum P.I., Gunn D.A., Ogilvy R.D. and Kuras O.; 2010: *Predicting the movements of permanently installed electrodes on an active landslide using time-lapse geoelectrical resistivity data only.* Geophys. J. Int., 183, 543-556, doi: 10.1111/j.1365-246X.2010.04760.x.

Corresponding author: Maysam Abedi
Petroleum Engineering and Geophysics Laboratory, School of Mining Engineering,
Faculty of Engineering, University of Tehran
Amirabad, Tehran 98, Iran
Phone: +98 21 61114563; e-mail: maysamabedi@ut.ac.ir